Electromagnetic Ion Cyclotron Waves in the Helium Branch Induced by Multiple Electromagnetic Ion Cyclotron Triggered Emissions

Masafumi Shoji, Yoshiharu Omura

Research Institute for Sustainable Humanosphere, Kyoto University, Uji,

Kyoto, JAPAN

Benjamin Grison

Institute of Atmospheric Physics AS CR Bocni II/14011, 14131 Praha 4,

Czech Republic

Jolene Pickett

Department of Physics and Astronomy, The University of Iowa, Iowa City,

IA, 52242, USA

Iannis Dandouras

IRAP, University of Toulouse, UPS-OMP, Toulouse, France

CNRS, IRAP, 9 Ave. Colonel Roche, BP 44346, F-31028 Toulouse cedex 4,

France

Mark Engebretson

Department of Physics, Augsburg College, 2211 Riverside Avenue,

Minneapolis, MN 55454, USA

Abstract.

Electromagnetic ion cyclotron (EMIC) triggered emissions with rising tones between the H^+ and He^+ cyclotron frequencies were found in the inner magnetosphere by the recent Cluster observations. Another type of EMIC wave with a constant frequency is occasionally observed below the He^+ cyclotron frequency after the multiple EMIC triggered emissions. We performed a self-consistent hybrid simulation with a one-dimensional cylindrical magnetic flux model approximating the dipole magnetic field of the Earth's inner magnetosphere. In the presence of energetic protons with a sufficient density and temperature anisotropy, multiple EMIC triggered emissions are reproduced due to the nonlinear wave growth mechanism of rising-tone chorus emissions, and a constant frequency wave in the He^+ EMIC branch is subsequently generated. Through interaction with the multiple EMIC rising-tone emissions, the velocity distribution function of the energetic protons is strongly modified. Because of the pitch angle scattering of the protons, the gradient of the distribution in velocity phase space is enhanced along the diffusion curve of the He^+ branch wave, resulting in the linear growth of the EMIC wave in the He^+ branch.

Masafumi Shoji and Yoshiharu Omura, Research Institute for Sustainable Humanosphere, Kyoto University, Gokasho, Uji, Kyoto 611-0011, Japan. (shouji@rish.kyoto-u.ac.jp)

1. Introduction

Electromagnetic ion cyclotron (EMIC) triggered emissions in the Earth's inner magnetosphere have been studied via Cluster observations [*Pickett et al.*, 2010; *Omura et al.,* 2010], theory [*Omura et al.,* 2010], and simulation [*Shoji and Omura,* 2011]. The observations [*Pickett et al.*, 2010] show that emissions have left-hand-polarized rising tone spectra in the ULF frequency range. They are triggered by Pc1 (EMIC) pulsations [e.g. *Troitskaya*, 1961; *Tepley*, 1961; *Roux et al.*, 1982; *Anderson et al.*, 1992a, 1992b; *Engebretson et al.*, 2007] around the equatorial region. The nonlinear growth theory derived by *Omura et al.* [2010] shows a good agreement with the observations in the frequency sweep rate of the rising tones. Moreover, the EMIC waves which propagate at a frequency below the H^+ cyclotron frequency play an important role for the cyclotron resonance interaction with the relativistic electrons of the radiation belts. *Meredith et al.* [2003] have performed statistical analyses on these interactions. The resonant quasi-linear scattering of energetic electrons by EMIC waves in the H^+ and He^+ branches have been theoretically analyzed by *Summers and Thorne* [2003] and *Summers et al.* [2007].

A hybrid simulation [*Shoji and Omura,* 2011] has successfully reproduced the EMIC triggered emissions in a cylindrical magnetic flux model assumed as the equatorial region of the Earth's inner magnetosphere. The duration, frequency sweep rate, and saturation level of the triggered emissions show a good agreement with the observations. In the simulation, the velocity distribution of the energetic protons is strongly modulated by formation of large proton holes due to the triggered emissions. Because of the inward motion of the proton holes due to the rising frequency of the triggered emissions, the

energetic protons are scattered over a wide range of velocities parallel to the background magnetic field.

In some cases of the observations and simulations, we can find EMIC waves below the He^+ cyclotron frequency after generation of the EMIC triggered emissions in the H^+ branch. We present a Cluster observation of the multiple triggered emissions and the EMIC waves in the He^+ branch in Section 2. In Section 3, we reproduce the multiple EMIC triggered emissions by a hybrid code simulation to clarify how the associated EMIC waves in the He^+ branch are excited by the triggered emissions. Section 4 gives a summary and discussion.

2. Observations

The full description of the wave properties of the observed triggered emissions is found in *Pickett et al.* [2010]. In Figure 1, we focus on a shorter time interval when the spacecraft is in the Northern Hemisphere. Flux Gate Magnetometer data are used in order to have a frequency range starting from DC, which includes a part of the spectrum below 0.8 Hz that was not displayed in Figure 2 of *Pickett et al.* [2010]. In the spectrogram (top panel of Figure 1), triggered emissions are detected between 08:05 and 08:15 UT (cf. *Pickett et al.* [2010] for general wave properties). The first riser (at 08:12) is the most intense. It is followed by several other less powerful risers. The two risers detected immediately after the first one have a shorter frequency extent (up to 2.4 Hz). The last one ends at 08:16, and despite its weak power, the emission rises to 3 Hz. Triggered emissions display a high level of coherence indicative of a high degree of polarization [*Santolik et al.*, 2003]. This observed coherence is much larger than that of the EMIC waves observed in the same time frame. The second part of the event, starting from 08:15, is dominated by

strong monochromatic emissions (at 0.7 Hz) just below the local helium gyrofrequency (black solid line). Weaker monochromatic emissions are also detected above the helium gyrofrequency around 1.4 and 2.2 Hz.

The time evolution of the velocity distribution function of the energetic protons at 08:12:04, 08:14:48, 08:15:04, and 08:17:08 UT is shown in Figures 2a, 2b, 2c, and 2d, respectively. Comparing Figures 2a with 2b, we find the pitch angle scattering of particles in a wide velocity range due to the drastic change of the resonance velocity of the triggered emission with rising frequencies (decreasing resonance velocity from the white dashed lines in Figure 2a to the white dash-dotted lines in Figure 2b). This wide pitch angle scattering shows good agreement with the simulation result in *Shoji and Omura* [2011]. The distributions shown in Figure 2c and 2d are characteristic of the period, following the triggered emissions, when monochromatic emissions are seen in Figure 1a for the H^+ (f ∼1.4 Hz) and He^+ ($f \sim 0.7$ Hz) branches. The resonance velocities of the H^+ branch waves are shown as black dashed lines in Figure 2c. The EMIC waves in the He^+ branch are observed around the time in Figure 2d. The resonance velocities of the He^+ branch wave are shown as black dash-dotted lines in Figure 2d. The energetic protons around these resonance velocities are scattered along the diffusion curves of these waves [*Gendrin* 1968]. The markers in magenta indicate velocities at which pronounced variations of the distribution are found.

3. Hybrid simulation

We have developed a one-dimensional (1D) hybrid code with a cylindrical magnetic flux model [*Shoji et al.,* 2009; *Shoji and Omura*, 2011]. We use the same model configuration as *Shoji and Omura* [2011]. According to the observational results [*Omura et al.*, 2010],

the cyclotron and the plasma frequencies of protons are assumed as 3.7 Hz and 353.4 Hz, respectively, at the magnetic equator. Thus the amplitude of the ambient magnetic field is B_{0eq} =243 nT, and the Alfven velocity is 443 km/s at the equator. The number of grids of the physical region taken along the x axis is $N_x = 4,096$ with the grid spacing $\Delta x = 0.1V_A/\Omega_H (= 1.9$ km), and the time step is $\Delta t = 0.004/\Omega_H (= 1.72 \times 10^{-4}$ s), where V_A and Ω_H are the Alfven velocity and the cyclotron frequency of the cold protons at the equator, respectively. The frequency and the wavenumber of the triggering waves, which are excited by the left handed polarized external current source, are taken from the observations as $(\omega_w, k_w) = (0.409\Omega_H, 0.27\Omega_H/V_A)$, which correspond to a frequency 1.5 Hz and a wavelength $(2\pi/k_w)$ 450 km. The wave amplitude of the triggering wave is $B_w = 0.25$ nT.

We assume four ion species. Cold plasma components of H^+, He^+ and O^+ are assumed, and the thermal distributions of them are neglected. The thermal velocities of energetic protons in the parallel and perpendicular directions are $0.002c$ and $0.00267c$, respectively, where c is the speed of light. The density of these ions are $0.729n_e$ $0.095n_e$, $0.095n_e$, and $0.081n_e$, respectively, where n_e (=178 /cc) is the density of the electron fluid. The charge-to-mass ratios of the protons, helium, oxygen are $1.0e/m_H$, $0.25e/m_H$, and $0.0625e/m_H$, respectively, where e and m_H are the elementary charge and mass of the proton, respectively. The average numbers of superparticles of cold H^+, He^+, O^+, and energetic H^+ in a cell are 256, 256, 256, and 16384, respectively. Their densities are assumed so that the wave dispersion relation gives the observed cut-off frequencies. Energetic H^+ ions with temperature anisotropy are introduced as resonant particles with EMIC waves, forming a loss cone distribution function [*Shoji and Omura,* 2011]. The quiet start [*Birdsall and*

Langdon, 1985] is used to reduce the initial thermal fluctuations. The energetic protons are initialized to form a spatial distribution that is stable in time with adiabatic motion in the parabolic magnetic field.

We separate the wave magnetic fields into forward and backward propagating wave components using the same method as used by *Shoji and Omura* [2011]. To obtain the dynamic spectra around the equatorial region, we apply a Fourier transform in a limited time window and slide it from the initial time to the end of the simulation period. The size of the window is chosen as $t \sim 11.2$ s for a sufficient resolution in the frequency domain. Figures 3a and 3b show the dynamic spectra of the magnetic field of the forward and backward propagating waves around the equatorial region, respectively. Because we introduced a higher density of energetic protons than that assumed in *Shoji and Omura* [2011], there still remains enough free energy to generate another triggered emission in the simulation space. We obtain multiple rising tone EMIC triggered emissions in the H^+ branch both in the forward and backward propagating waves as shown in Figure 3. A substantial part of the distribution function of the protons is scattered by the first triggered emission [*Shoji and Omura*, 2011], and thus the second triggered wave saturates faster than the first one. The multiple chorus emissions are discussed by *Katoh and Omura* [2011], and the same dependency of the multiple emissions on the energetic particle density is also found in the case of EMIC triggered emissions. From $t \sim 30$ s, after the second triggered emission starts, another branch of EMIC waves below the He^+ cyclotron frequency (0.925 Hz, shown by the white dashed lines) is generated both in forward and backward propagating wave spectra. These spectra show a good agreement with the observation shown in Figure 1.

Figures 4a to 4f show the velocity distribution functions of the energetic protons around the equatorial region at different times. We focus on the negative velocity range of the distribution function interacting with the forward propagating waves. In Figure 4g, we calculate a value ΔE which is defined as (energy density in the velocity phase space) $\times$ (density gradient along the diffusion curve of the EMIC wave in the He^+ branch). When ΔE is positive, the energetic protons around the resonance velocity are scattered losing their energy, and thus the He^+ branch EMIC waves can be generated. We also plot the resonance velocities V_{R0} of the triggering wave, $V_{\rm He}$ of EMIC waves in the He^+ branch, and V_R of the triggered waves in Figures 4a to 4f. Here, we note that these velocities satisfy

$$|V_{Rf}| < |V_{\rm He}| < |V_{R0}| \quad , \tag{1}$$

where V_{Rf} indicates the resonance velocity of the triggered waves at the highest frequency. Through the nonlinear wave growth, a proton hole is generated around the resonance velocity V_R [*Shoji and Omura*, 2011] and it moves inward to the core part of the distribution functions. The resonance velocity of triggered waves V_R changes from V_{R0} and approaches to V_{Rf} due to the nonlinear process.

Figure 4a shows the initial distribution function. From the initial time to around $t \simeq 16$ s, because the resonance velocity of the first triggered wave $|V_R|$ is greater than $|V_{\rm He}|$, the density gradient along the diffusion curve of the He^+ branch wave is enhanced at a higher pitch angle of the distribution function and thus the value of ΔE takes a positive value. As the frequency of the triggered emission increases, $|V_R|$ becomes smaller and moves across $V_{\rm He}$ as shown in Figure 4b. As shown in Figure 4b, a proton hole is formed around the resonance velocity of the first triggered emission (white solid line), which is near $V_{\rm He}$

(black dashed line), the density increases in the lower pitch angles, and thus the value of ΔE starts to decrease. After that, as the depth of the proton hole becomes larger, there appears a negative ΔE region as shown in Figure 4c. Through the inward motion of the proton holes, the core part of the distribution function is scattered [*Shoji and Omura*, 2011]. Because a substantial number of protons are scattered in the region $|v| < |V_{\rm He}|$, the density gradients are enhanced around $V_{\rm He}$ along the diffusion curve of the He^+ branch wave as shown in Figure 4c. At $t = 20.1$ s in Figure 4g, we find a positive value region of ΔE. However, there still remains a negative region and thus the He^+ branch waves are not generated. The same process also takes place with the second triggered emission.

The resonance velocity of the second emission, shown by a purple line, also moves across $V_{\rm He}$ as shown in Figure 4d. As a result of this scattering due to the multiple triggered emissions, a broad positive ΔE appears around $t = 30.1$ s in Figure 4g. The corresponding unstable distribution function is shown in Figure 4e. The EMIC waves in the He^+ branch start to be generated at this time as shown in Figure 3. Energetic protons near the resonance velocity of the wave in the He^+ branch lose their energy. Therefore, the EMIC waves in the He^+ branch are generated through the cyclotron resonance with the energetic protons. After the generation of the He^+ branch waves, due to the scattering of the distribution functions by the He^+ branch EMIC waves, the velocity distribution becomes flat along the diffusion curve of the wave as shown in Figure 4f.

4. Summary and Discussion

We performed a hybrid simulation for multiple EMIC triggered emissions, and found that EMIC waves in the He^+ branch are induced by the triggered emissions. With a sufficient flux of energetic protons in the simulation space, the multiple EMIC triggered

emissions are generated through nonlinear wave growth from the triggering waves [*Omura et al.,* 2010; *Shoji and Omura*, 2011]. With the rising tone EMIC triggered emissions, the resonance velocities of the triggered emissions move across that of the He^+ branch waves. The distribution function is modulated so as to enhance the density gradient along the diffusion curve of the He^+ branch waves. Thus, the He^+ branch EMIC waves are generated after the multiple EMIC triggered emissions in the H^+ branch. EMIC waves with slightly lower frequency in the H^+ branch are also found in the simulation result. The H^+ branch waves have a resonance velocity greater than that of the triggering wave. Thus, the H^+ branch waves are generated through cyclotron resonance with the energetic protons scattered from the phase space volume interacting with the triggered emissions in the distribution function. These EMIC waves in the H^+ and He^+ branches are generated through the linear growth processes independently. The generation of these waves shows a good agreement with the observations shown in Figure 1.

Based on the simulation results shown in Figure 4, we can interpret the time evolution of the distribution functions observed by the Cluster spacecraft shown in Figure 2. Comparing Figures 2b with 2a, we find the pitch angle scattering of the core part of the distribution function. The particles in the lower parallel velocities are scattered through the inward motion of the proton holes due to the rising frequencies. Some of the energetic protons are scattered to a velocity greater than the resonance velocity of the triggering wave, and the EMIC waves in the H^+ branch are generated at a slightly lower frequency ~ 1.4 Hz. The energetic protons are precipitated into the loss cone around the resonance velocities of the H^+ branch waves as we can see in Figure 2c. A density gradient also appears along the diffusion curve of the He^+ branch waves. The He^+ branch waves are

generated and the phase space in the lower pitch angle and lower parallel velocity is filled by the scattered protons as shown in Figure 2d.

In the observations shown in Figure 1, we find more EMIC triggered emissions than in the simulation. These multiple triggered emissions should be caused by injections of energetic protons into the inner magnetosphere. As a result, the amplitude of the He^+ branch waves becomes larger. In the observation shown in Figure 1, we find the lower H^+ branch wave is 1.4 Hz, while He^+ branch wave is 0.8 Hz. The three wave coupling process induces a wave at 2.2 Hz (=1.4 Hz + 0.8 Hz), which is not a simple harmonic of the He^+ branch wave. A hybrid simulation with continuous injection of fresh energetic protons is left as a future study.

Acknowledgments. Computation in the present study was performed with the KDK system of Research Institute for Sustainable Humanosphere and Academic Center for Computing and Media Studies at Kyoto University as a collaborative research project. The present study was supported in part by a Grant-in-Aid for Research Fellows from the Japan Society for the Promotion of Science, and Grant-in-Aid 20340135 of the Ministry of Education, Science, Sports and Culture of Japan. The authors thank the Cluster Active Archive (CAA) website for supplying the high resolution FGM data. BG acknowledges support of grant GACR P209/11/P848. JP acknowledges support from NASA GSFC under Grant NNX11AB38G. ME acknowledges support at Augsburg College from U. S. National Science Foundation Grant ATM-0827903 and Dragos Constantinescu of the Technical University of Braunschweig for his support in preparing the data.

References

Anderson, B. J., R. E. Erlandson, and L. J. Zanetti (1992a), A statistical study of Pc 1 - 2 magnetic pulsations in the equatorial magnetosphere: 1. Equatorial occurrence distributions, *J. Geophys. Res., 97*, 3075.

Anderson, B. J., R. E. Erlandson, and L. J. Zanetti (1992b), A statistical study of Pc 1 - 2 magnetic pulsations in the equatorial magnetosphere: 2. Wave properties, *J. Geophys. Res., 97*, 3089.

Birdsall, C. K., and A. B. Langdon (1985), Plasma physics via computer simulation, *McGraw-Hill*.

Engebretson, M. J., et al. (2007), Cluster observations of Pc 1 - 2 waves and associated ion distributions during the October and November 2003 magnetic storms, *Planet. Space Sci., 55*, 829.

Gendrin, R. (1968), Pitch angle diffusion of low energy protons due to gyroresonant interaction with hydromagnetic waves, *J. Atmos. Terr. Phys. 30*, 1,313.

Katoh, Y., and Y. Omura (2011), Amplitude dependence of frequency sweep rates of whistler mode chorus emissions, *J. Geophys. Res., 116*, A07201.

Meredith, N. P., R. M. Thorne, R. B. Horne, D. Summers, B. J. Fraser, and R. R. Anderson (2003), Statistical analysis of relativistic electron energies for cyclotron resonance with EMIC waves observed on CRRES, *J. Geophys. Res., 108*, 1250.

Omura, Y., J. Pickett, B. Grison , O. Santolik, I. Dandouras, M. Engebretson, P. M. E Decreau, and A. Masson (2010), Theory and observation of electromagnetic ion cyclotron chorus emissions in the magnetosphere, *J. Geophys. Res., 115*, A07234.

Pickett, J. S., B. Grison, Y. Omura, M. J. Engebretson, I. Dandouras, A. Masson, M. L. Adrian, O. Santolik, P. M. E. Decreau, N. Cornilleau-Wehrlin, and D. Constantinescu (2010), Cluster observations of EMIC triggered emissions in association with Pc1 waves near Earth's plasmapause, *Geophys. Res. Lett., 37*, L09104.

Reme, H., et al. (2001), First multispacecraft ion measurements in and near the Earth's magnetosphere with the identical Cluster ion spectrometry (CIS) experiment, *Ann. Geophys., 19*, 1303-1354.

Roux, A., S. Perraut, J. Rauch, C. de Villedary, G. Kremser, A. Korth, and D. Young (1982), Wave - particle interactions near Ω_{He} observed on board GEOS 1 and 2: 2. Generation of ion cyclotron waves and heating of He+ ions, *J. Geophys. Res., 87*, 8174.

Santolik, O., D. A. Gurnett, J. S. Pickett, M. Parrot, and N. Cornilleau - Wehrlin (2003), Spatio - temporal structure of storm - time chorus, *J. Geophys. Res., 108(A7)*, 1278.

Shoji, M., Y. Omura, B. T. Tsurutani, O. P. Verkhoglyadova, and B. Lembege (2009), Mirror instability and L-mode electromagnetic ion cyclotron instability: Competition in the Earth's magnetosheath, *J. Geophys. Res., 114*, A10203.

Shoji, M., and Y. Omura (2011), Simulation of electromagnetic ion cyclotron triggered emissions in the Earth's inner magnetosphere, *J. Geophys. Res.*, 116, A05212.

Summers, D., B. Ni, and N. P. Meredith (2007), Timescales for radiation belt electron acceleration and loss due to resonant wave - particle interactions: 2. Evaluation for VLF chorus, ELF hiss, and electromagnetic ion cyclotron waves, *J. Geophys. Res.*, 112, A04207.

Summers, D., and R. M. Thorne (2003), Relativistic electron pitch-angle scattering by electromagnetic ion cyclotron waves during geomagnetic storms, *J. Geophys. Res., 108*

(A4), 1143.

Tepley, L. R. (1961), Observations of hydromagnetic emissions, *J. Geophys. Res., 66*, 1651.

Troitskaya, V. A. (1961), Pulsations of the earth's electromagnetic field with periods of 1 to 1.5 seconds and their connection with phenomena in the high atmosphere, *J. Geophys. Res., 66*, 5.

Figure 1. Dynamic power spectrum of the magnetic field (top panel) from DC to 3.5 Hz between 0805 and 0825 on March 30th, 2002 (data from the Flux Gate Magnetometer (FGM) onboard Cluster 4). The coherence level (bottom panel) is estimated for the most energetic part of the spectrogram. Spacecraft Magnetic Local Time and Magnetic Latitude are given for each time mark. The arrows indicate the times corresponding to Figures 2a, 2b, 2c, and 2d.

Figure 2. Velocity distribution functions of the high - energy component (40 eV to 40 keV) of protons in the $V_{\parallel} - V_{\perp}$ plane observed by the CIS-CODIF instrument of Cluster 4 [*Reme et al.*, 2001] at (a) 08:12:04, (b) 08:14:48, (c) 08:15:04, and (d) 08:17:08 UT on 30 March 2002. The white regions indicate the outside of the detectable region (90 km/s to 2770 km/s) or the region where no particles have been detected. The white dashed lines in panel (a), the white dash-dotted lines in panel (b), the black dashed lines in panel (c), and the black dash-dotted lines in panel (d) show the resonance velocities of the triggering waves, the triggered waves reaching the maximum frequency ($\sim$3 Hz), the H^+ branch waves with slightly lower frequency ($\sim$ 1.4 Hz), and the He^+ branch waves, respectively. The magenta markers show the regions where the distribution functions are changed.

Figure 3. Dynamic spectra of the magnetic fields of (a) forward propagating waves with triggering wave and (b) backward propagating waves with triggering wave. The black and white dashed lines show the frequency of the triggering waves and the cyclotron frequency of He^+, respectively.

Figure 4. Velocity distribution functions of energetic protons at (a) $t = 0$ s, (b) $t = 15.1$ s, (c) $t = 20.1$ s, (d) $t = 25.1$ s, (e) $t = 30.1$ s, and (f) $t = 79.7$ s normalized by the maximum value of the initial velocity distribution function f_{0M}. The black dashed line, white dashed line, white solid line, and purple solid line show the resonance velocities of EMIC wave in the He^+ branch, the triggering wave, the first EMIC triggered wave, and the second triggered wave, respectively. The black solid curves show the diffusion curves [*Gendrin* 1968] of the EMIC waves in the He^+ branch. (g) The kinetic energy density gradient in phase space ΔE along the diffusion curve at the resonance velocity V_{He} in arbitrary units.

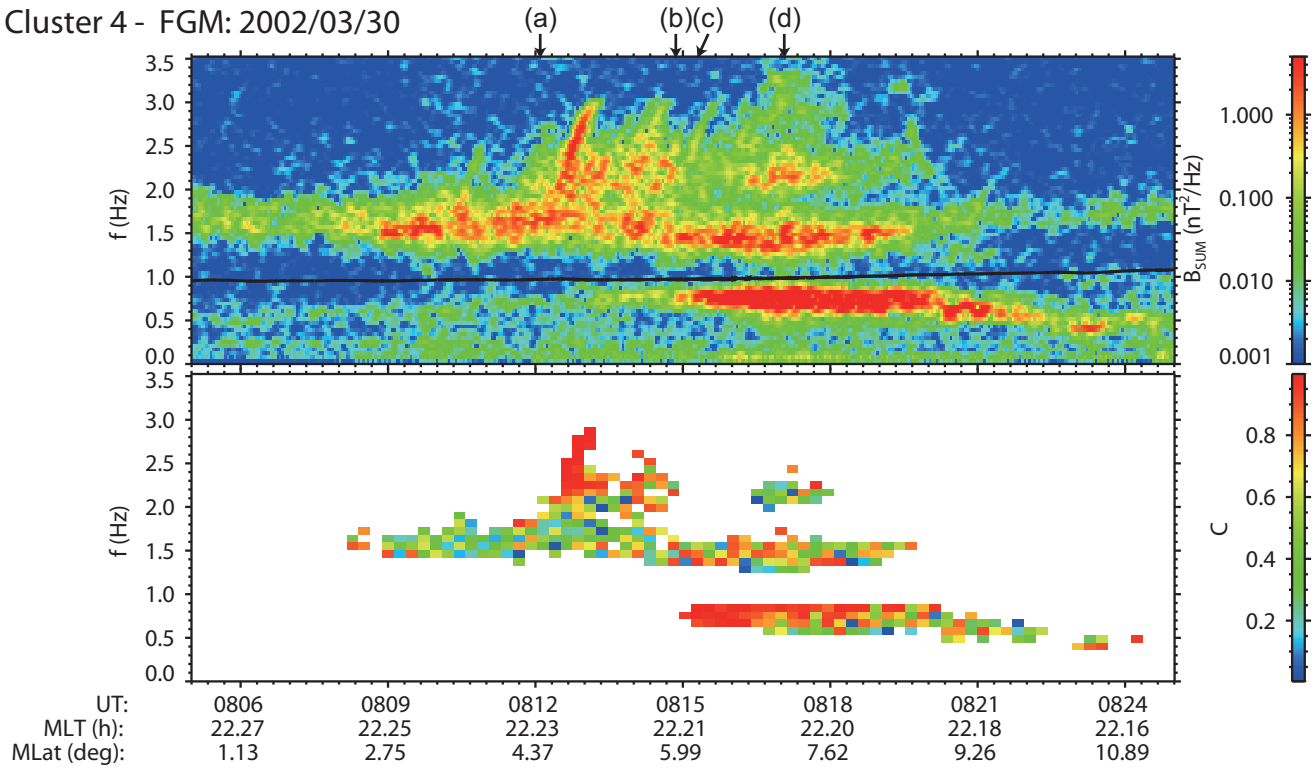

Figure 1. Dynamic power spectrum of the magnetic field (top panel) from DC to 3.5 Hz between 0805 and 0825 on March 30th, 2002 (data from the Flux Gate Magnetometer (FGM) onboard Cluster 4). The coherence level (bottom panel) is estimated for the most energetic part of the spectrogram. Spacecraft Magnetic Local Time and Magnetic Latitude are given for each time mark. The arrows indicate the times corresponding to Figures 2a, 2b, 2c, and 2d.

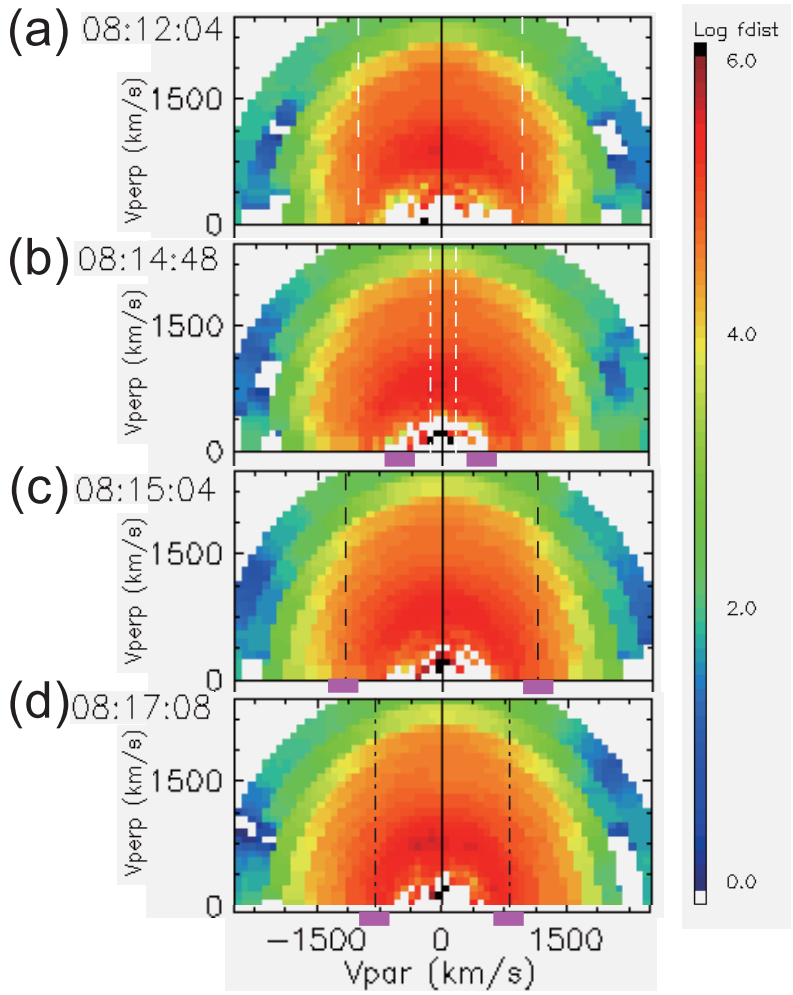

Figure 2. Velocity distribution functions of the high - energy component (40 eV to 40 keV) of protons in the $V_{\parallel} - V_{\perp}$ plane observed by the CIS-CODIF instrument of Cluster 4 [*Reme et al.*, 2001] at (a) 08:12:04, (b) 08:14:48, (c) 08:15:04, and (d) 08:17:08 UT on 30 March 2002. The white regions indicate the outside of the detectable region (90 km/s to 2770 km/s) or the region where no particles have been detected. The white dashed lines in panel (a), the white dash-dotted lines in panel (b), the black dashed lines in panel (c), and the black dash-dotted lines in panel (d) show the resonance velocities of the triggering waves, the triggered waves reaching the maximum frequency (∼3 Hz), the H^+ branch waves with slightly lower frequency (∼ 1.4 Hz), and the He^+ branch waves, respectively. The magenta markers show the regions where the distribution functions are changed.

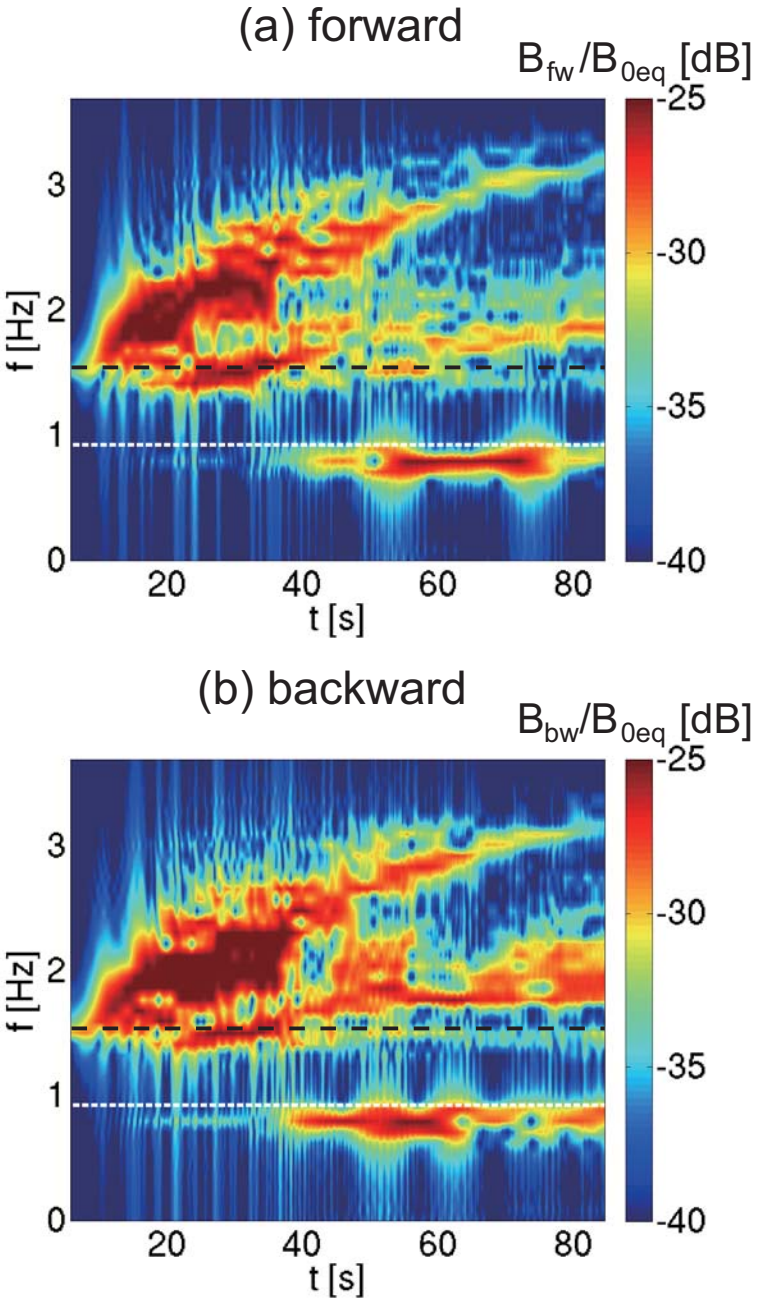

Figure 3. Dynamic spectra of the magnetic fields of (a) forward propagating waves with triggering wave and (b) backward propagating waves with triggering wave. The black and white dashed lines show the frequency of the triggering waves and the cyclotron frequency of He^+, respectively.

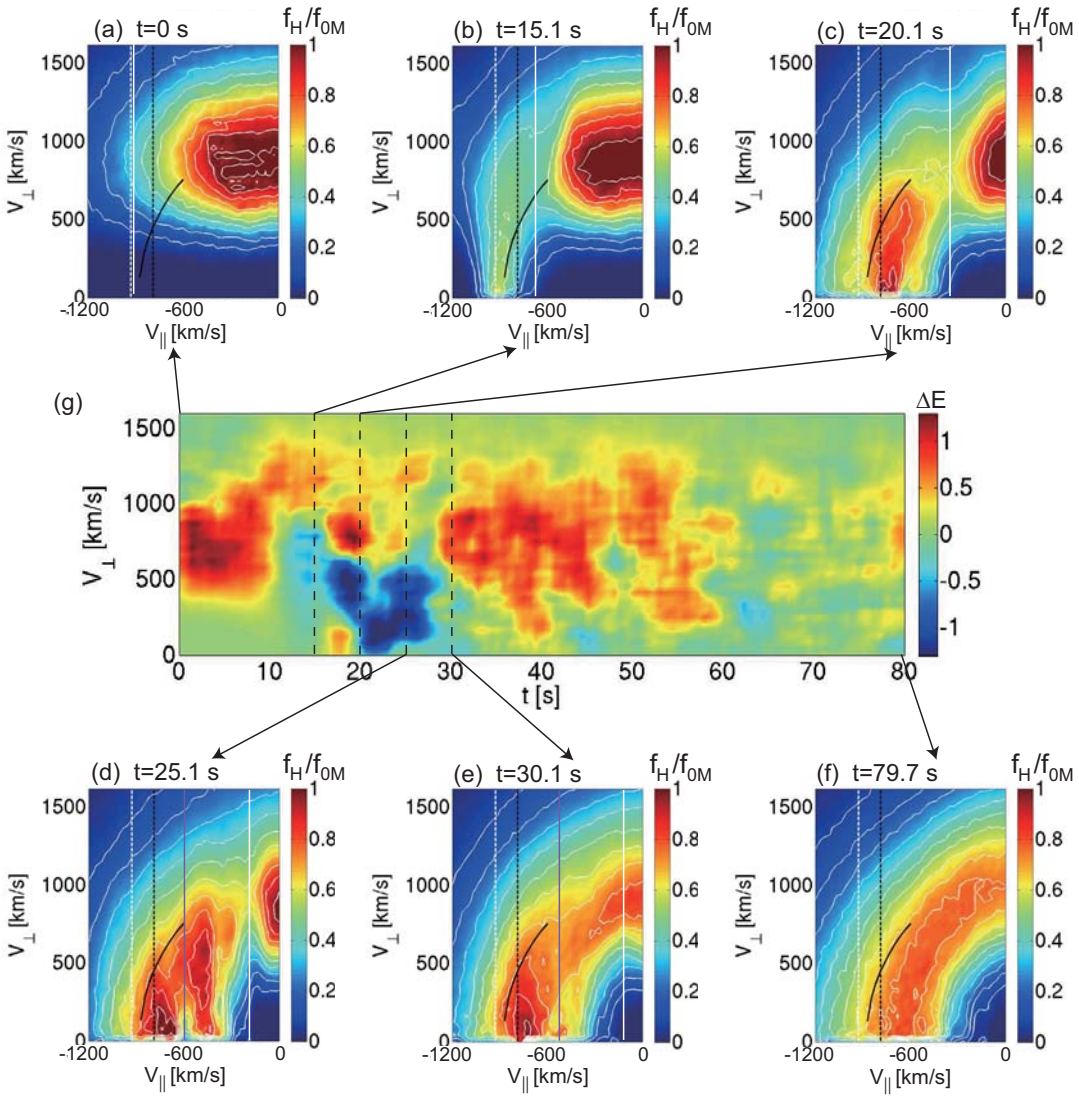

Figure 4. Velocity distribution functions of energetic protons at (a) $t = 0$ s, (b) $t = 15.1$ s, (c) $t = 20.1$ s, (d) $t = 25.1$ s, (e) $t = 30.1$ s, and (f) $t = 79.7$ s normalized by the maximum value of the initial velocity distribution function f_{0M}. The black dashed line, white dashed line, white solid line, and purple solid line show the resonance velocities of EMIC wave in the He^+ branch, the triggering wave, the first EMIC triggered wave, and the second triggered wave, respectively. The black solid curves show the diffusion curves [*Gendrin* 1968] of the EMIC waves in the He^+ branch. (g) The kinetic energy density gradient in phase space ΔE along the diffusion curve at the resonance velocity V_{He} in arbitrary units.